IEEE Photonics Journal
An IEEE Photonics Society Publication

Open Access

Monitoring the Etching Process of Hi-Bi Fiber Through a Fiber Loop Mirror

Volume 9, Number 6, December 2017

Danling Wu
Jun Zhu
Hui Wang
Benli Yu

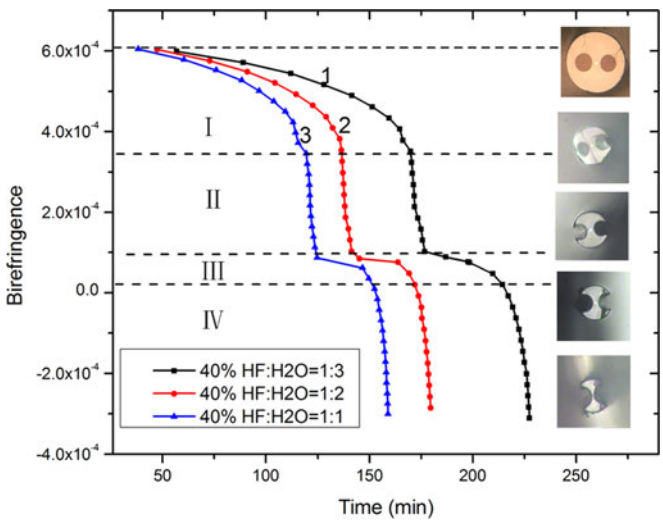

DOI: 10.1109/JPHOT.2017.2760889
1943-0655 © 2017 IEEE

IEEE photonics SOCIETY

IEEE

Monitoring the Etching Process of Hi-Bi Fiber Through a Fiber Loop Mirror

Danling Wu, Jun Zhu, Hui Wang, and Benli Yu

Key Laboratory of Opto-Electronic Information Acquisition and Manipulation, Ministry of Education, Anhui University, Hefei 230601, China

DOI:10.1109/JPHOT.2017.2760889

Manuscript received August 11, 2017; revised October 1, 2017; accepted October 3, 2017. Date of publication October 10, 2017; date of current version October 26, 2017. This work was supported in part by the National Key Research and Development Program under Grant 2016YFC0301900, in part by the University Science Research Project of Anhui Province under Grant KJ2016A793, and in part by the Key Research and Development Project of Anhui Province under Grant 1704a0902061. Corresponding author: Jun Zhu (e-mail: zhuj@ahu.edu.cn).

Abstract: A method for monitoring the etching process of Hi-Bi fiber is proposed and demonstrated. The birefringence of the etching fiber is accurately calculated by tracking the shift of the interference spectrum in a high-birefringence fiber loop mirror interferometer. Then, the degree of etching can be inferred by the relationship between the etching-fiber birefringence and the fiber structure. A section of PANDA fiber is used as an example to experimentally demonstrate the proposed method. The results show that the calculated birefringence is consistent with the theoretical simulation. Furthermore, four different structural states, which reflected in four different rate of change, are presented in the whole etching process of PANDA fiber. This method has the advantages of easy realization, high precision, and repeatability, and it can be used in the preparation of Hi-Bi microfiber photonic devices.

Index Terms: Etching process, Hi-Bi fiber, birefringence, fiber loop mirror.

1. Introduction

Microfiber photonic devices have attracted numerous research interests recently since they can serve strong coupling of propagating optical evanescent fields. Optical sensors based on these devices have special advantages including faster response, higher sensitivity, low power consumption, light weight and outstanding mechanical flexibilities. A series of related studies were reported, including optical near-field image [1], [2], biochemistry [3], [4], biomedicine [5], [6] and environment monitoring [7], [8] *et al.* The manufacturing method of these devices is important for further practical applications. Some micromachining methods, such as heat-pulling [9]– [11], laser ablation [12], [13], requires expensive equipment and complicated manipulation. In comparison, chemical etching methods [14]–[17] are used more widely because of the low cost and simple operation. For example, Simon Pevec *et al.* proposed a nWG FPI production from a method used for an in-line evanescent field access device production based on chemical etching [17], and some other interesting work based on chemical etching methods [18], [19]; Tarun Kumar Gangopadhyay *et al.* developed an evanescent field access block (EAB) sensor with an etched single mode fiber used to detection of chemicals [4].

In chemical etching applications, it is necessary to accurately monitor the etching process for excellent microfiber structure. In the traditional methods, controlling the etching concentration and

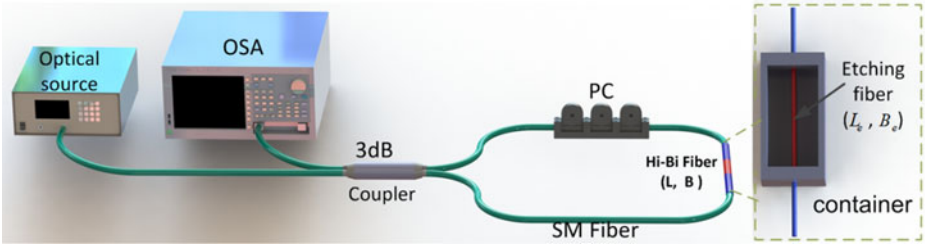

Fig. 1. Structure of Hi-Bi FLM and experimental setup of etch fiber. Where PC is polarization controller and OSA is optical spectrum analyzer.

the etching time are usually used in order to obtain different fiber diameter [15]– [17], but it is easy to be influenced by surrounding temperature and etching solution density. Recently, several methods were presented for monitoring the fiber etching process real time. Tao miaomiao *et al.* monitored the process of fabricating optical fiber probe nanotips by combining a fiber optic spectrometer with chemical etching [20]. O. Frazão structured optical fiber loop mirror used for monitoring the fiber diameter through the analysis of wavelength spacing changing of the fringe minima [14].

In this paper, a method for monitoring optical fiber etching process by tracking the shift of the interference spectrum in a high birefringence fiber loop mirror (Hi-Bi FLM) interferometer is presented and experimentally demonstrated. The relationship between the spectral change and the etching-fiber birefringence, which can reflect the characteristics of etching-fiber structure, is proposed. In experiment, the calculated birefringence is consistent with the theoretical simulation, when etching the PANDA fiber cladding. Furthermore, four different structural states are presented, when continue to etching the PANDA fiber. Compared with traditional methods, this method can eliminate the impact of surrounding temperature and etching solution density. It can increase its potential for the preparation of high precision fiber optic evanescent field structure.

2. Theoretical Analysis

Fig. 1 shows the traditional structure of Hi-Bi FLM. The incident light is split into c1ockwise and counterclockwise beams by the 3 dB coupler, and the two beams pass through the Hi-Bi fiber from opposite directions to produce phase difference. When the two beams are transmitted for one cycle, the interference occurs in the coupling region of the 3 dB coupler. The polarization controller is used to adjusted polarization states of light. The expression for transmissivity is given by [21]

$$T = \frac{1}{2}\left(1 + \cos\frac{2\pi BL}{\lambda}\right) \tag{1}$$

Where B, L are birefringence and length of Hi-Bi fiber, respectively, λ is wavelength of optical source. As shown in Fig. 1, a section of Hi-Bi fiber will be etched, assuming that the length is L_e, the birefringence variation of the etching-fiber is ΔB. Thus (1) can be rewritten as

$$T = \frac{1}{2}\left(1 + \cos\frac{2\pi\left(BL - \Delta BL_e\right)}{\lambda}\right) \tag{2}$$

Fig. 2 shows the simulation results from (1) and (2), the interference spectra will move to the left or right during etching. Assuming one spectral dip λ_k of the order of interference k moves to λ'_k, while the adjacent dip moves from λ_{k-1} to λ'_{k-1}. According to (1) and (2), we can deduce a set of equations:

$$\begin{cases} \frac{2\pi BL}{\lambda_k} = (2k + 1)\pi \\ \frac{2\pi(BL - \Delta BL_e)}{\lambda'_k} = (2k + 1)\pi \\ \frac{2\pi(BL - \Delta BL_e)}{\lambda'_{k-1}} = (2k - 1)\pi \end{cases} \tag{3}$$

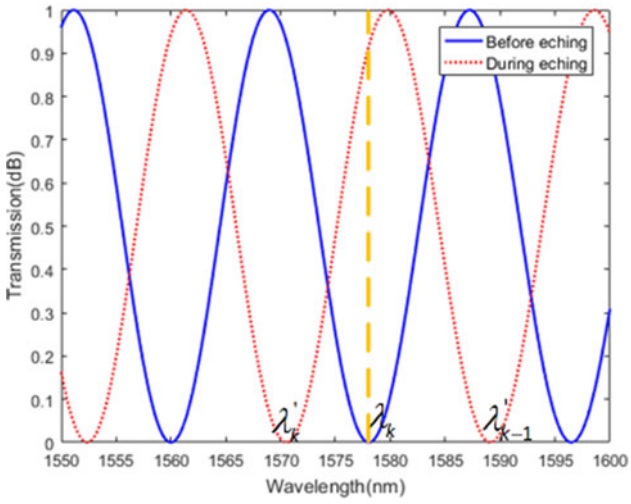

Fig. 2. Spectral response of the Hi-Bi FLM before and during etching.

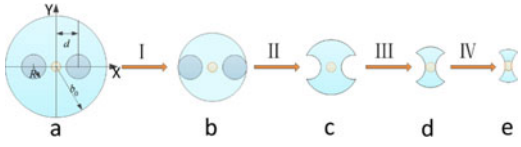

Fig. 3. Illustration of PANDA fiber etching process.

The relationship between ΔB and wavelength of spectral dips can be written as:

$$\Delta B = \frac{\lambda'_{k-1}}{L_e} \frac{\lambda_k - \lambda'_k}{\lambda'_{k-1} - \lambda'_k} \tag{4}$$

When interference spectrum moves one cycle, the λ'_{k-1} is equal to λ_k, (4) can be simplified as follows:

$$\Delta B^1 = \frac{\lambda_k}{L_e} \tag{5}$$

The change of the etching-fiber birefringence is a constant value. We can choose and mark one spectral dip of initial transmission spectrum as a reference wavelength, then tracking the shift of the interference spectrum in etching. So the etching-fiber birefringence can be calculated from the following equation:

$$B_e = B - N\Delta B^1 - \Delta B \tag{6}$$

where N is the difference of the order of interference through the reference wavelength during the etching process. Equation (6) shows that we can monitor the etching-fiber birefringence in real time by recording the spectral shift. Since the birefringence is closely related to the structure of the etching fiber, we can use the method to monitor the optical fiber etching process. In the following, a section of PANDA fiber is employed as an example to analyze the regularity between the etching-fiber structure and the birefringence changes in etching process.

As shown in Fig. 3(a), the PANDA fiber is composed of cladding, stress applying parts (SPAs) and core. The circular B-doped SPAs are symmetrically distributed on both sides of the fiber core. In the etching process, the etch rate will vary depending on the material. In general, it will be divided into four stages, as shown in Fig. 3.

Stage I corresponds to Fig. 3(a) and (b), only the fiber cladding is etched. The fiber at this stage can still be seen as stress-induced fiber because the SAPs are still there. The birefringence of the

fiber can be given [20]

$$B = \frac{2CE\Delta\alpha\Delta T}{1-\nu}\left(\frac{R}{d}\right)^2\left[1-3\left(\frac{d}{b}\right)^4\right] \tag{7}$$

Where E, C, ν are the Young's modulus, the stress-optic coefficient and the Poisson ratio of the optical fiber, respectively, $\Delta\alpha$ is the difference of the thermal expansion coefficients between the cladding and the SAPs, ΔT is the temperature difference between the room temperature and softening temperature of the pure silica glass. Moreover, R, b, d respectively is the radius of SAP, the radius of cladding, the distance from the center of SAP to the core.

When the fiber is etching, the radius of cladding is gradually reduced, assuming that the initial value is b_0, the reduction rate is a_1, so $b = b_0 - a_1 \times t$. Let $a_0 = \frac{2CE\Delta\alpha\Delta T}{1-\nu}$, the etching-fiber birefringence can be written as,

$$B_e = a_0\left(\frac{R}{d}\right)^2\left[1-3\left(\frac{d}{b_0-a_1 t}\right)^4\right] \tag{8}$$

Stage II corresponds to Fig. 3(b) and (c). Due to the influence of B-doped materials in SAPs, which could break the silicate network structure [23], it causes an obviously difference in etch rate between the SAPs and pure silica in some etching solutions such as hydrofluoric acid (HF) at this stage. Similar techniques are often used to manufacture microstructure fiber sensors [24], [25]. Therefore, we can obtain the special structure with no-SAPs as shown in Fig. 3(c). It can be seen that the stress in this fiber is completely released. The birefringence of the fiber should be only caused by the geometry and surrounding refractive index difference.

Stage III corresponds to Fig. 3(c) and (d). In this process, both X and Y direction are pure silica cladding, the etching-fiber is getting thinner with similar geometric shape, and the evanescent field in the X direction will be higher than the Y direction. This kind of structure still has a significant birefringence.

Stage IV is the last stage corresponds to Fig. 3(d) and (e), the X direction has been etched to the germanium doped core, which etched at a higher rate than the pure silica in HF. This is a key stage to obtain high precision fiber optic evanescent field structure, because the optical evanescent field in X direction is getting stronger and stronger in etching process. Furthermore, we can still monitor the optical fiber etching process in this stage by measuring the change of etching-fiber birefringence.

In general, during the etching process, the structure of the etching-PANDA-fiber will be changed continuously and present four different structural states, meanwhile, the etching-fiber birefringence, which can be calculated by tracking the shift of the interference spectrum in a Hi-Bi FLM interferometer, will also change with the structure. That means if we can track the shift of the interference spectrum, we can monitor the optical fiber etching process. This method could eliminate the impact of surrounding temperature and etching solution density, and could be applied to other types of Hi-Bi fibers.

3. Experiment and Results

Fig. 1 illustrates the experimental setup that consists of an amplified spontaneous emission source (ASE-CL, 1526-1602 nm), an optical spectrum analyzer (OSA, AQ6370C, YOKOGAWA) with a maximum resolution of 20 pm, a Hi-Bi FLM and a container with etchant. A section of PANDA fiber (PM15-1-2, CETC-46) is inserted into the fiber loop to form a Hi-Bi FLM.

Firstly, the relationship between the etching-fiber birefringence and the theoretical values derived from (8) in stage I in the etching process is studied. The cross section of the PANDA fiber is shown in Fig. 4. The initial radius of fiber $b_0 = 62.5\,\mu$m, the radius of stress region $R = 16.5\,\mu$m, and the distance between stress region and fiber center $d = 25.5\,\mu$m.

In order to calibrate the etch rate a_1 in (8), Several samples of the PANDA fibers are placed in container with etchant (40%HF:H2O = 1:3) and taking them out at predetermined time intervals

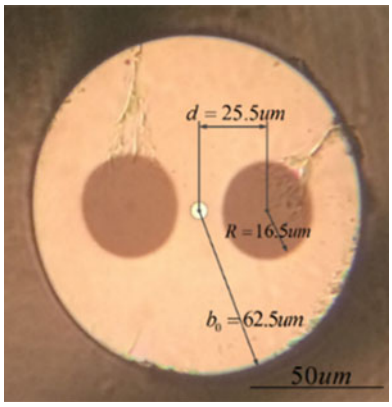

Fig. 4. The cross section of the PANDA fiber.

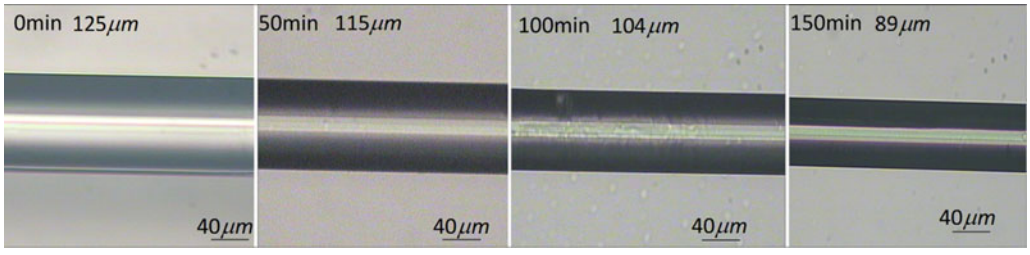

Fig. 5. The diameter of the PANDA fiber at different etching time.

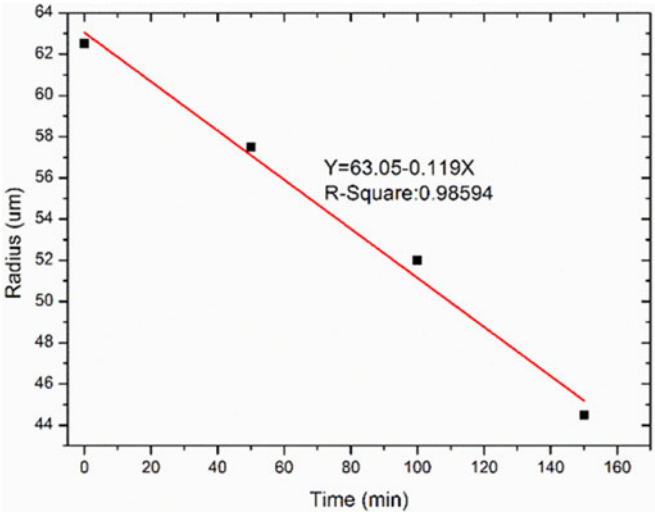

Fig. 6. Radius of the fiber dropped as a function of the time.

(50 min) in room temperature. Then the diameter of the PANDA fiber during the etching is measured as in Fig. 5. We can obtained the etch rate $a_1 = 0.119\,\mu\text{m}/\text{min}$, as shown in Fig. 6

Then, a section of the same type of PANDA fiber is inserted into the fiber loop, as shown in Fig. 1. The length of the whole Hi-Bi fiber $L = 18.8$ cm, where the length of the etching-fiber $L_e = 5.7$ cm. Fig. 7 shows the spectral response of the Hi-Bi FLM before and during etching. It can be seen that the spectrum has moved and the wavelength spacing has changed in the etching process. The initial birefringence of the PANDA fiber can be calculated by the initial spectrum as $B_0 = 6.2655E - 4$. According to (7), the factor $a_0 = 0.00167$. Then, the shifts of the spectrum in the etching process

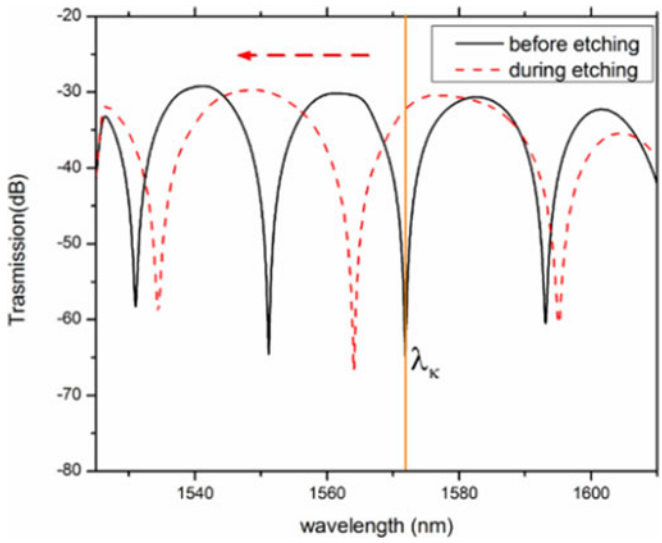

Fig. 7. Interference spectra of the refractometer before and during chemical etching.

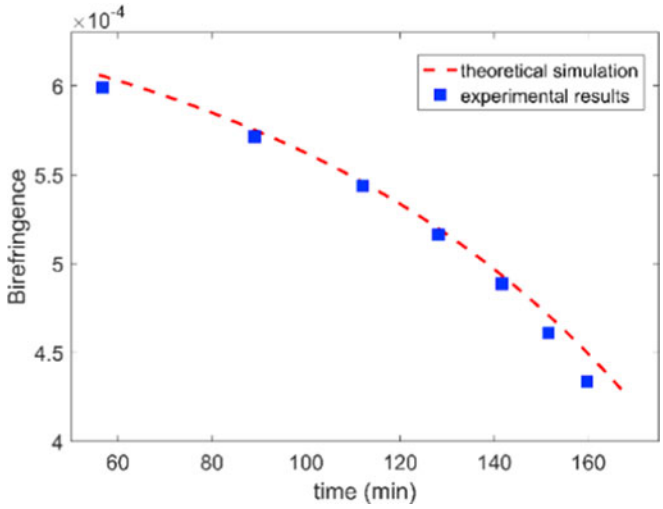

Fig. 8. Experimental and theoretical comparison of the birefringence of the optical fiber and the etching time.

are recorded which can calculate the etching-fiber birefringence by (6). The relationship between the etching-fiber birefringence in experiment and the simulation of (8) is shown in Fig. 8.

Fig. 8 corresponds to the stage I in above analysis. The experimental results are in good agreement with the theoretical simulation, which means that it is possible to reflect the structural characteristics of the etching-fiber by monitoring the birefringence during the etching process.

We continue to etch this fiber in order to verify the other stages of the etching process. The result is shown in curve 1 of Fig. 9. It can be seen that, during the whole etching process, the rate of change of the birefringence shows four obviously states which are slow-fast-slow-fast, corresponding to the four stages in the theoretical analysis. In stage I and III, the structure of etching-fiber changes slowly because only pure silica was etched, so the birefringence changes slowly. Correspondingly, in stage II and IV, due to the doped materials, the etch rate in some directions is faster, the structure of etching-fiber changes faster, resulting in a faster change of birefringence. The fiber cross section on the right side in Fig. 9 shows that the above analysis is correct.

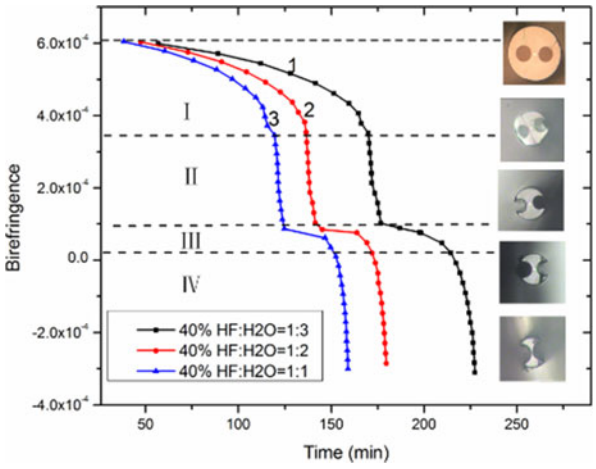

Fig. 9. Left: the relationship between the birefringence and the etching time in the different concentration etchant; right: Microscope images of cross section of the etching fiber.

In order to get more relationships between the birefringence and the structural characteristics of the etching-fiber, we use different etchant concentration to complete the above experiment. The results are shown in Fig. 9, curve 2 and curve 3 correspond to different etch densities, respectively. It can be seen that the etching process is significantly faster, but there are still exist the four obviously states, and more importantly, the etching-fiber birefringence at each critical point of the change in etch rate are equal to the results of curve 1. Furthermore, through the observation of the fiber cross section, they are the same too.

From the experimental analysis, the etching-fiber birefringence is closely related to its structural change during the etching process. Although studies have shown that temperature may also influences the etching-fiber birefringence [26], but it should be very small when compared with the birefringence changes cause by etching. In particular, when the B-doped SPAs are etched, the influence of temperature can be negligible. Therefore, it can be considered that during the etching process, the etching-fiber birefringence is in a one-to-one relationship with its structure. This method effectively solves various uncertainties in the traditional etching methods by controlling the etching concentration and the etching time and provides a feasible solution for obtain high precision fiber optic evanescent field structure.

4. Conclusion

We proposed a method for monitoring optical fiber etching process by tracking the shift of the interference spectrum in a Hi-Bi FLM. A section of PANDA fiber is used as an example to experimentally demonstrate the method. During the etching process, four different structural states by monitoring the etching-fiber birefringence were presented. This method only needs to obtain the interference spectrum formed by the phase difference between the fast axis and the slow axis of Hi-Bi fiber. So it can be applied to other types of Hi-Bi fibers, such as Bow-Tie fiber, elliptical-core fiber, etc. and some other loop configurations with output port probe [27], which is considered to be more valuable in sensing applications [28], [29]. This method has the advantages of easy realization, high precision and repeatability, increasing its potential for the preparation of high precision fiber optic evanescent field structure.

References

[1] G. S. Athanasiou *et al.*, "Toward mid-infrared, subdiffraction, spectral-mapping of human cells and tissue: SNIM (scanning near-field infrared microscopy) tip fabrication," *J. Lightw. Technol.*, vol. 34, no. 4, pp. 1212–1219, Feb. 2016.

[2] Y. Yang, H. Chai, C. Li, Y. Zhang, F. Wu, and J. Bai, "Surface defects evaluation system based on electromagnetic model simulation and inverse-recognition calibration method," *Opt. Commun.*, vol. 390, pp. 88–98, May 2017.
[3] C. C. Meek and P. Pantano, "Spatial confinement of avidin domains in microwell arrays," *Lab Chip*, vol. 1, pp. 158–63, Dec. 2001.
[4] T. K. Gangopadhyay, A. Giorgini, A. Halder, M. Pal, M. C. Paul, and S. Avino, "Detection of chemicals using a novel fiber-optic sensor element built in fiber loop ring-resonators," *Sensors Actuators B, Chem.*, vol. 206, pp. 327–335, 2015.
[5] J. M. Tam, L. Song, and D. R. Walt, "DNA detection on ultrahigh-density optical fiber-based nanoarrays," *Biosensors Bioelectron.*, vol. 24, pp. 2488–2493, Apr. 2009.
[6] S. Sridevi, K. S. Vasu, S. Asokan, and A. K. Sood, "Sensitive detection of C-reactive protein using optical fiber Bragg gratings," *Biosensors Bioelectron.*, vol. 65, pp. 251–256, Mar. 2015.
[7] A. M. Cardenas-Valencia, R. H. Byrne, M. Calves, L. Langebrake, D. P. Fries, and E. T. Steimle, "Development of stripped-cladding optical fiber sensors for continuous monitoring - II: Referencing method for spectral sensing of environmental corrosion," *Sensors Actuators B, Chem.*, vol. 122, pp. 410–418, Mar. 2007.
[8] E. Angelini, S. Grassini, D. Mombello, A. Neri, M. Parvis, and G. Perrone, "Plasma modified POF sensors for in situ environmental monitoring of museum indoor environments," *Appl. Phys. A, Mater. Sci. Process.*, vol. 100, pp. 975–980, Sep. 2010.
[9] A. Felipe, G. Espindola, H. J. Kalinowski, J. A. S. Lima, and A. S. Paterno, "Stepwise fabrication of arbitrary fiber optic tapers," *Opt. Exp.*, vol. 20, pp. 19893–19904, Aug. 2012.
[10] D. D. Hudson, E. C. Maegi, A. C. Judge, S. A. Dekker, and B. J. Eggleton, "Highly nonlinear chalcogenide glass micro/nanofiber devices: Design, theory, and octave-spanning spectral generation," *Opt. Commun.*, vol. 285, pp. 4660–4669, Oct. 2012.
[11] N.-K. Chen, Y.-H. Hsieh, and Y.-K. Lee, "Tapered fiber Mach-Zehnder interferometers for vibration and elasticity sensing applications," *Opt. Exp.*, vol. 21, pp. 11209–11214, May 2013.
[12] V. R. Machavaram, R. A. Badcock, and G. F. Fernando, "Fabrication of intrinsic fibre Fabry-Perot cavities in silica optical fibres via F-2-laser ablation," *Meas. Sci. Technol.*, vol. 18, pp. 928–934, Mar. 2007.
[13] W. Jin, C. Wang, H. Xuan, and W. Jin, "Tunable comb filters and refractive index sensors based on fiber loop mirror with inline high birefringence microfiber," *Opt. Lett.*, vol. 38, pp. 4277–4280, Nov. 2013.
[14] O. Frazão, A. Guerreiro, J. L. Santos, and J. M. Baptista, "Birefringence monitoring of a Hi-Bi fibre under chemical etching through a fibre loop mirror," *Meas. Sci. Technol.*, vol. 18, pp. N81–N83, Oct. 2007.
[15] H. Kbashi, "Fabrication of submicron-diameter and taper fibers using chemical etching," *J. Mater. Sci. Technol.*, vol. 28, pp. 308–312, Apr. 2012.
[16] J. C. Mikkelsen and J. K. S. Poon, "Microdroplet-etched highly birefringent low-loss fiber tapers," *Opt. Lett.*, vol. 37, pp. 2601–2603, Jul. 2012.
[17] S. Pevec and D. Donlagic, "Nanowire-based refractive index sensor on the tip of an optical fiber," *Appl. Phys. Lett.*, vol. 102, 2013, Art. no. 213114.
[18] S. Pevec, E. Cibula, B. Lenardic, and D. Donlagic, "Micromachining of optical fibers using selective etching based on phosphorus pentoxide doping," *IEEE Photon. J.*, vol. 3, no. 4, pp. 627–632, Aug. 2011.
[19] S. Pevec and D. Donlagic, "Miniature micro-wire based optical fiber-field access device," *Opt. Exp.*, vol. 20, pp. 27874–27887, Dec. 2012.
[20] M. Tao, Y. Jin, N. Gu, and L. Huang, "A method to control the fabrication of etched optical fiber probes with nanometric tips," *J. Opt.*, vol. 12, Dec. 2010, Art. no. 015503.
[21] A. N. Chryssis, S. M. Lee, S. B. Lee, S. S. Saini, and M. Dagenais, "High sensitivity evanescent field fiber Bragg grating sensor," *IEEE Photon. Technol. Lett.*, vol. 17, no. 6, pp. 1253–1255, Jun. 2005.
[22] K.-H. Tsai, K.-S. Kim, and T. F. Morse, "General solutions for stress-induced polarization in optical fibers," *J. Lightw. Technol.*, vol. 9, no. 1, pp. 7–17, Jan. 1991.
[23] G. A. C. M. Spierings, "Wet chemical etching of silicate glasses in hydrofluoric acid based solutions," *J. Mater. Sci.*, vol. 28, pp. 6261–6273, 1993.
[24] E. Preter, B. Preloznik, V. Artel, C. N. Sukenik, D. Donlagic, and A. Zadok, "Monitoring the evaporation of fluids from fiber-optic micro-cell cavities," *Sensors*, vol. 13, pp. 15261–15273, Nov. 2013.
[25] S. Pevec and D. Donlagic, "Miniature fiber-optic sensor for simultaneous measurement of pressure and refractive index," *Opt. Lett.*, vol. 39, pp. 6221–6224, Nov. 2014.
[26] E. De la Rosa, L. A. Zenteno, A. N. Starodumov, and D. Monzon, "All-fiber absolute temperature sensor using an unbalanced high-birefringence Sagnac loop," *Opt. Lett.*, vol. 22, pp. 481–483, Apr. 1997.
[27] O. Frazao, R. M. Silva, and J. L. Santos, "High-birefringent fiber loop mirror sensors with an output port probe," *IEEE Photon. Technol. Lett.*, vol. 23, no. 2, pp. 103–105, Jan. 2011.
[28] T. Hu, Y. Zhao, and D. Wu, "Novel torsion sensor using a polarization maintaining photonic crystal fiber loop mirror," *Instrum. Sci. Technol.*, vol. 44, pp. 46–53, 2015.
[29] Y. Zhao, T. T. Song, D. Wu, and Q. Wang, "Research on fiber optic temperature sensor using a novel high-birefringent fiber loop mirror with a reflection probe," *Sensors Actuators A, Phys.*, vol. 184, pp. 22–27, Sep. 2012.